Biochimica et Biophysica Acta 1843 (2014) 544–553

Contents lists available at ScienceDirect

Biochimica et Biophysica Acta

journal homepage: www.elsevier.com/locate/bbamcr

Analysis of α3 GlyR single particle tracking in the cell membrane

Kristof Notelaers [a,b], Susana Rocha [b], Rik Paesen [a], Nick Smisdom [a], Ben De Clercq [a], Jochen C. Meier [c], Jean-Michel Rigo [a], Johan Hofkens [b], Marcel Ameloot [a,*]

[a] Biomedical Research Institute, Hasselt University and School of Life Sciences, Transnational University Limburg, Agoralaan gebouw C, 3590 Diepenbeek, Belgium
[b] Laboratory for Photochemistry and Spectroscopy, Department of Chemistry, Katholieke Universiteit Leuven, Celestijnenlaan 200F, B-3001 Heverlee, Belgium
[c] RNA Editing and Hyperexcitability Disorders Group, Max Delbrück Center for Molecular Medicine, Robert-Rössle-Strasse 10, 13092 Berlin, Germany

ARTICLE INFO

Article history:
Received 30 August 2013
Received in revised form 22 November 2013
Accepted 25 November 2013
Available online 4 December 2013

Keywords:
Glycine receptor
Alpha3 subunit
RNA splicing
Single particle tracking
Confined motion
Directed motion

ABSTRACT

Single particle tracking (SPT) of transmembrane receptors in the plasma membrane often reveals heterogeneous diffusion. A thorough interpretation of the displacements requires an extensive analysis suited for discrimination of different motion types present in the data. Here the diffusion pattern of the homomeric α3-containing glycine receptor (GlyR) is analyzed in the membrane of HEK 293 cells. More specifically, the influence of the α3 RNA splice variants α3K and α3L on lateral membrane diffusion of the receptor is revealed in detail. Using a combination of ensemble and local SPT analysis, free and anomalous diffusion parameters are determined. The GlyR α3 free diffusion coefficient is found to be 0.13 ± 0.01 $\mu m^2/s$ and both receptor variants display confined motion. The confinement probability level and residence time are significantly elevated for the α3L variant compared to the α3K variant. Furthermore, for the α3L GlyR, the presence of directed motion was also established, with a velocity matching that of saltatory vesicular transport. These findings reveal that α3 GlyRs are prone to different types of anomalous diffusion and reinforce the role of RNA splicing in determining lateral membrane trafficking.

1. Introduction

The trafficking of proteins after insertion in the cell membrane is crucial for cell homeostasis and functionality [1–3]. Rudimentary movement of membrane proteins is governed by Brownian motion and can be modeled as diffusion in a 2D fluid plane [4]. The corresponding diffusion coefficient is dependent on the temperature, the radius of the membrane-spanning segment and the membrane viscosity [5,6]. Diffusion is a stochastic process, yet several cellular mechanisms exist which are capable of steering protein movement in the cell membrane [7–10]. The movement of proteins susceptible to these mechanisms deviates from normal diffusion and is termed anomalous diffusion [11–13]. Deviations from normal diffusion can signify either a restriction of protein diffusion in space or non-random travel of proteins along an imposed path. The former is termed sub-diffusion, hindered diffusion or confined motion, while the latter is termed super-diffusion, flow or directed motion [14–17].

Anomalous diffusion is frequently revealed when studying the dynamics of membrane proteins [18,19]. Especially the increasing application of Single Particle Tracking (SPT) has furthered the understanding of protein trafficking in the membrane [20,21]. SPT has given access to nanometer accuracy on millisecond time-scales, allowing the monitoring of fast protein dynamics with high spatial resolution [22–25]. When monitoring a transmembrane receptor in a complex biological system, it is important to correctly represent and quantify the SPT data. Therefore, many efforts have already gone into the representation of SPT data and determination of an appropriate diffusion model [16,26,27].

In synaptic biology, anomalous diffusion of membrane proteins has been monitored extensively using SPT [28]. Effective neurotransmission requires neurotransmitter receptors to be located at the post-synaptic membrane and a turnover of these receptors to maintain sensitivity [29–31]. These properties impose a strong regulation of neurotransmitter receptor trafficking and lateral mobility. For many neurotransmitter receptors, interacting proteins have been identified which form scaffolds or chaperones [32–36]. In order to elucidate the nature of these interactions, accurate quantification of receptor diffusion is crucial [37,38].

The glycine receptor (GlyR) is a neurotransmitter receptor of the cys-loop ligand-gated ion channel (LGIC) family [39]. It functions as a pentameric chloride channel, leading to developmentally regulated neuronal hyperpolarisation upon activation [40,41]. The GlyR α3 has attracted significant attention as it is involved in inflammatory pain sensitization [42]. Nevertheless, little is known about the molecular basis governing membrane diffusion of the GlyR α3. From the *GLRA3*-

Abbreviations: SPT, Single particle tracking; GlyR, Glycine receptor; LGIC, Ligand gated ion channel; TM, Transmembrane segment; HEK 293, Human embryonic kidney 293; MSD, Mean square displacement; TIRF, Total internal reflection fluorescence

* Corresponding author at: Agoralaan gebouw C, 3590 Diepenbeek, Belgium. Tel.: +32 11 26 92 33; fax: +32 11 26 92 99.
E-mail address: marcel.ameloot@uhasselt.be (M. Ameloot).

0167-4889/$ – see front matter © 2013 Elsevier B.V. All rights reserved.
http://dx.doi.org/10.1016/j.bbamcr.2013.11.019

gene transcript, two α3-subunit variants are generated via post-transcriptional processing [43]. These variants are identified as the short α3 K and long α3 L GlyR, with the latter containing an extra 15 amino acid insert in the large intracellular loop between transmembrane segments 3 and 4 (TM 3–4). This protein region is instrumental to receptor trafficking and regulation of synaptic localization [44], receptor desensitization [43] and channel gating [45]. In the hippocampus of patients with temporal lobe epilepsy, GlyR α3 RNA processing is changed [44,46,47]. Detailed knowledge about the (anomalous) diffusion properties of the GlyR α3 RNA splice variants and how they function and dysfunction will advance our understanding of pathogenic mechanisms in epilepsy and inflammatory pain sensitization.

In previous work, a variety of nano- and micro-fluorimetric techniques were used to characterize homomeric α3 GlyR diffusion and aggregation on multiple time and length scales [48]. The results showed RNA splice variant dependent aggregation of α3 GlyRs, accompanied by differential diffusion dynamics. The measurements done on short time and length scales, especially by SPT, indicated that the differential diffusion dynamics are associated with anomalous diffusion. The results showed the putative presence of confined GlyR α3 motion, with additional directed motion for α3 L. In this work, the GlyR α3 anomalous diffusion is verified and quantified by focusing on the SPT analysis. After determination of the free diffusion coefficient, confined and directed motion were identified by local displacement analysis [49,50]. This was based on respectively the displacement size and the asymmetry of the trajectories. By providing a detailed view on GlyR α3 motion in the cell membrane, valuable insights on RNA splicing dependent dynamics are acquired.

2. Materials and methods

2.1. Single particle tracking

Single particle tracking experiments were executed as described elsewhere [48]. Briefly, transient transfection of HEK 293 cells by calcium phosphate co-precipitation was used for the expression of HA-tagged α3K and α3L splice variants of the mouse GlyR α3. After 24 h the receptors were labeled using a polyclonal anti-HA antibody directly labeled with Alexa 647. Images of the bottom membrane were acquired at 10 Hz using total internal reflection fluorescence (TIRF)-microscopy with an EM-CCD camera, while the cells were incubated at 37 °C. Particle detection, trajectory reconstruction and all consequent analysis were performed by in-house developed MATLAB® (R2010b, The Mathworks, Gouda, The Netherlands) routines. Only particle trajectories with at least 16 consecutive displacements were considered and the average localization precision (σ) was 18 nm. In subsequent analysis immobile trajectories were not removed and σ was kept fixed.

2.2. Ensemble displacement analysis

In order to quantify GlyR diffusion on the ensemble level, the mean square displacement (MSD) was determined from the cumulative distributions of square displacements over consecutive time lags. A single-component function failed to accurately describe the data and therefore fitting was done with a two-component function (see supp. mat. S1) [51]:

$$P\left(r^2,t\right)=1-\sum_{i=1,2}A_i\exp\left(-\frac{r^2}{r_i^2}\right)\quad\sum_{i=1,2}A_i=1 \tag{1}$$

For each time lag this equation yields two MSD (r^2) with $r_1^2 > r_2^2$ and two respective fractions (A_1, A_2). Fitting of the first component was done with a linear function, representing a free diffusion model, yielding D_e:

$$\left\langle r^2\right\rangle = 4D_e t + 4\sigma^2 \tag{2}$$

For the second component a non-linear model was used, representing an anomalous diffusion model, yielding a transport factor D_e' and anomalous exponent α_e:

$$\left\langle r^2\right\rangle = 4D_e' t^{\alpha_e} + 4\sigma^2 \tag{3}$$

In case of $\alpha_e < 1$ the particle undergoes sub-diffusion, in case of $\alpha_e > 1$ the particle is subjected to super-diffusion.

2.3. Local displacement analysis

To determine sections of trajectories displaying confined or directed motion, each trajectory was analyzed in a sliding segment fashion. The sliding window parameters for section identification are scaled to the minimum number of time lags in a trajectory ($N = 16$). Parameter values for confined and directed motion identification are selected based on the nature of the respective anomalous process, as further explained below. The final thresholds were selected based on detecting ≤0.1% anomalous displacements in the simulated data (see suppl. mat. S2).

2.4. Confined motion

In order to detect confined motion, the method as described by Simson R. *et al.* was applied [50]. To this end the cumulative probability $\Psi(R,t)$, *i.e.* the probability of a diffusing particle staying in a region R as a function of time t, was determined as follows [52]:

$$\log(\Psi) = 0.2048 - 2.5117 Dt/R^2 \tag{4}$$

The parameter D_e from the ensemble displacement analysis was used as an estimate for D. R^2 was determined for each segment as the maximum squared displacement from the initial point of that segment. The time span of the sliding segment was 8 time lags ($t = 0.8$ s), which gave robust averaging for even the shortest trajectories. The confinement probability was transformed into a confinement probability level (L_c) according to:

$$L_c = \begin{cases} -\log(\Psi)-1 & \Psi \le 0.1 \\ 0 & \Psi > 0.1 \end{cases} \tag{5}$$

For each displacement, an individual L_c was determined by averaging over all segments containing the displacement. In order to be considered as a confinement region, a minimum of 10 consecutive displacements were required to have $L_c > 1.6$, corresponding to $\Psi(R,t) = 0.0025$. Each confinement region was quantified by the radius (ρ) of the smallest circle enclosing all corresponding confined displacements and the *residence time* was determined by the time span of the confined trajectory section.

2.5. Directed motion

Directed motion was identified by analyzing the asymmetry of the ellipse of gyration [53], calculated over segments of 6 time lags. This was chosen as a compromise between averaging and short time scale sensitivity. The asymmetry parameter (a_2), becomes 0 for linear trajectories and 1 for circular trajectories and is calculated as follows:

$$a_2 = R_2^2/R_1^2 \tag{6}$$

with R_1^2 and R_2^2 being the major and minor eigenvalues, respectively, of the radius of gyration tensor (**T**) calculated from the x and y positions of the particle throughout the segment:

$$T = \begin{pmatrix} \frac{1}{N}\sum_{j=1}^{N}\left(x_j-\langle x\rangle\right)^2 & \frac{1}{N}\sum_{j=1}^{N}\left(x_j-\langle x\rangle\right)\left(y_j-\langle y\rangle\right) \\ \frac{1}{N}\sum_{j=1}^{N}\left(x_j-\langle x\rangle\right)\left(y_j-\langle y\rangle\right) & \frac{1}{N}\sum_{j=1}^{N}\left(y_j-\langle y\rangle\right)^2 \end{pmatrix} \quad (7)$$

The cumulative probability of a_2 ($\Pr(a_2)$) occurring for a randomly diffusing particle was interpolated from values given by Saxton M.J.[52]. A directed motion probability level (L_d) was calculated for values of a_2 within the provided range of $\Pr(a_2)$:

$$L_d = \begin{cases} -\log(\Pr(a_2)) - 0.3578 & \Pr(a_2) \le 0.43871 \\ 0 & \Pr(a_2) > 0.43871 \end{cases} \quad (8)$$

An individual L_d for each displacement was determined, by averaging over all segments containing the displacement. In order for a section to be considered as directed motion, a minimum of 7 consecutive displacements were required to have $L_d > 1.52$, corresponding to $\Pr(a_2) = 0.0132$. Furthermore, asymmetrical displacements also exhibiting confinement ($L_c > 1.6$) were eliminated. Finally, the resulting sections were required to show a net square displacement exceeding the mean square displacement given by the time span of the section and D_e (Eq. (2)). The quantification of the identified directed motion was done by calculating the *distance*, *travel time* and speed of the directed motion sections. The *distance* was determined by the sum of all first order displacements. The *travel time* was determined by the time span. The *speed* was obtained by dividing *distance* by *travel time*.

The *prevalence* of confined and directed motion was determined by the percentage of trajectories displaying the respective motion type. Furthermore, for confined motion, the *confined fraction* is determined by the percentage of confined displacements. A displacement is considered confined only when it belongs to a confined trajectory section.

2.6. Statistics

The individual output parameters reported in this work are represented either by showing the full distribution and/or the mean with standard error. The full distributions are made up by grouping all values for the corresponding parameter over all experiments from a single expression system. The range reported for each distribution is the 1st to the 99th percentile. Unless stated otherwise, the mean with standard error for a parameter is calculated by averaging the mean parameter value from each individual experiment (n) for a single expression system. For the α3 K-variant 7 cells were measured ($n = 7$) generating 1629 trajectories, while for the α3 L-variant 9 cells were measured ($n = 9$) generating 4291 trajectories. Statistically significant differences were evaluated by means of a t-test.

3. Results

The influence of RNA splicing on GlyR α3 biophysical membrane behavior was investigated by analyzing separate SPT measurements of both splice variants α3 K and α3 L. First multi-component ensemble analysis was performed to assess the possible presence of anomalous diffusion and to determine the free diffusion coefficient. Next a local displacement analysis was applied to detect individual deviations from free diffusion, incorporating the previously determined value of the free diffusion coefficient. The presence of both confined and directed motion is established and quantified. In a last step, the coincidence of these two motion types was evaluated.

3.1. Multi-component ensemble analysis

The α3 K GlyR square displacement distribution for each individual experiment could be accurately fit with a two-component function for consecutive time lags (Eq. (1)). The first component showed a linear relationship between the MSD and time over consecutive time lags. This was characterized by a free diffusion model with $D_e = 0.13 \pm 0.01$ μm²/s according to Eq. (2) (Fig. 1A). The MSD of the second component could only be fitted with an anomalous diffusion model, according to Eq. (3). The recovered parameters were $\alpha_e = 0.62 \pm 0.06$ and $D_e' = (5.0 \pm 0.5) \times 10^{-3}$ μm²/s$^{\alpha}$ (Fig. 1B). The fractions are stable on the time scale of the analysis and reveal that the fraction of the

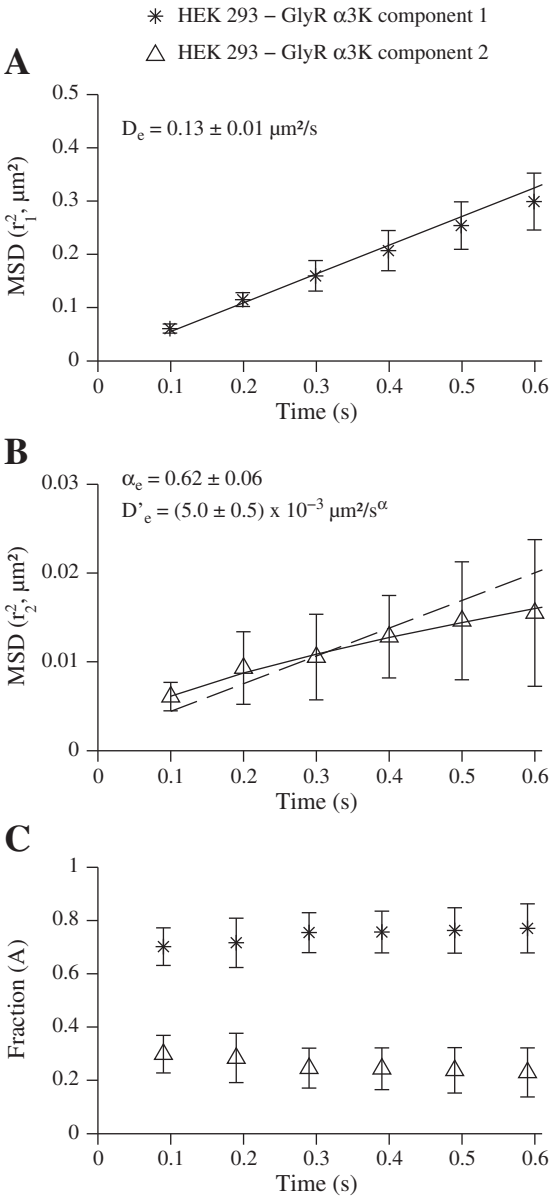

Fig. 1. Ensemble displacement analysis of GlyR α3 K diffusion in HEK 293. A two-component function (Eq. (1)) was used, yielding two MSDs ($r_1^2 > r_2^2$) with their respective fractions (error bars represent standard deviation). **A**. The MSD of the first component over consecutive time lags. A free diffusion model (Eq. (2), full line) was applied to determine the diffusion coefficient (D_e, indicated with 95% confidence interval). **B**. The MSD of the second component over consecutive time lags. A free diffusion model was not suitable for quantification (dotted line). Instead an anomalous diffusion model was applied (Eq. (3), full line), with α_e characterizing the deviation from normal diffusion (α_e and D_e' indicated with 95% confidence interval). **C**. The relative fractions of each component in the ensemble population.

first component dominates over that of the second component (Fig. 1C). In case of the α3 L square displacement distribution, a two-component function did not accurately describe the data. Using a three-component function improved fitting, yielding a first component with $D_e = 0.09 \pm 0.01$ μm²/s according to Eq. (2) (see suppl. mat. S3). Given that in theory, the free diffusion coefficient for both variants should be similar, we decided to use D_e from α3 K GlyRs as the standard for free diffusion of α3 GlyRs. Moreover, using D_e from the α3 L GlyR had little impact on the subsequent local displacements analysis (see suppl. mat. S4).

3.2. Local displacement analysis

In order to identify local deviations from normal diffusion, all trajectories were analyzed over a sliding window. Within the sliding window, the local displacement properties were calculated and compared to values expected for free diffusion. The analysis aimed at detecting both confined motion and directed motion. Confined motion was defined by regions where the receptors resided longer than expected for free diffusion. In order to identify these regions, L_c was determined, based on the ratio of the local maximum square displacement and D_e from the ensemble analysis (Fig. 2A). In order to determine directed motion, the trajectory form was evaluated by the asymmetry of the gyration matrix **T**, used to calculate L_d (Fig. 2B). In order for a trajectory section to be recognized as true directed motion, a minimum square displacement was also required.

In order to visualize the results from the local displacement analysis, first a section of the membrane is selected (Fig. 3). Plotting the trajectories in a color scheme indicating free diffusion (black), confined motion (red) or directed motion (green) shows that for the α3K variant (117 tracks) there is mainly free diffusion with occasional entry to the confined state. For α3L (223 tracks) on the other hand, confined motion is dominant, resulting in very localized trajectories covering only a small area of the membrane. Free diffusion and directed motion of this variant mainly occur around the areas of confinement (Fig. 3A). Fig. 3B shows the appearance of confined and directed motion in time. Sections of confined (circles) or directed motion (lines) are represented by color coding according to the central frame of the occurrence. The markers do not reflect the exact spatial dimensions. However, it becomes clear, especially for the L-variant, that some membrane areas contain multiple events spaced in time (black rectangles). Furthermore the occurrences of the anomalous diffusion events are spread out over the full timescale of the recording. Mapping of L_c indicates that the more frequent occurrence of confined motion for α3L is also coupled to higher values of L_c (Fig. 3C). When observing the spatial pattern of L_c for α3L, small high intensity interspersed peaks can be observed (red rectangles). Interestingly these areas show strong overlap with membrane areas containing reoccurring confined motion.

In order to visualize the dynamics creating the irregular patterns of L_c in areas with reoccurring confined events, trajectories and L_c were mapped for short time intervals. This illustrates that steep gradients in confinement strength are found in the motion of individual trajectories, a phenomenon which can occur for several receptors in the same area (e.g. red box) spaced over time. The trajectories in these areas show a high presence of confined motion, occasionally transitioning to or from free diffusion or directed motion (Fig. 4).

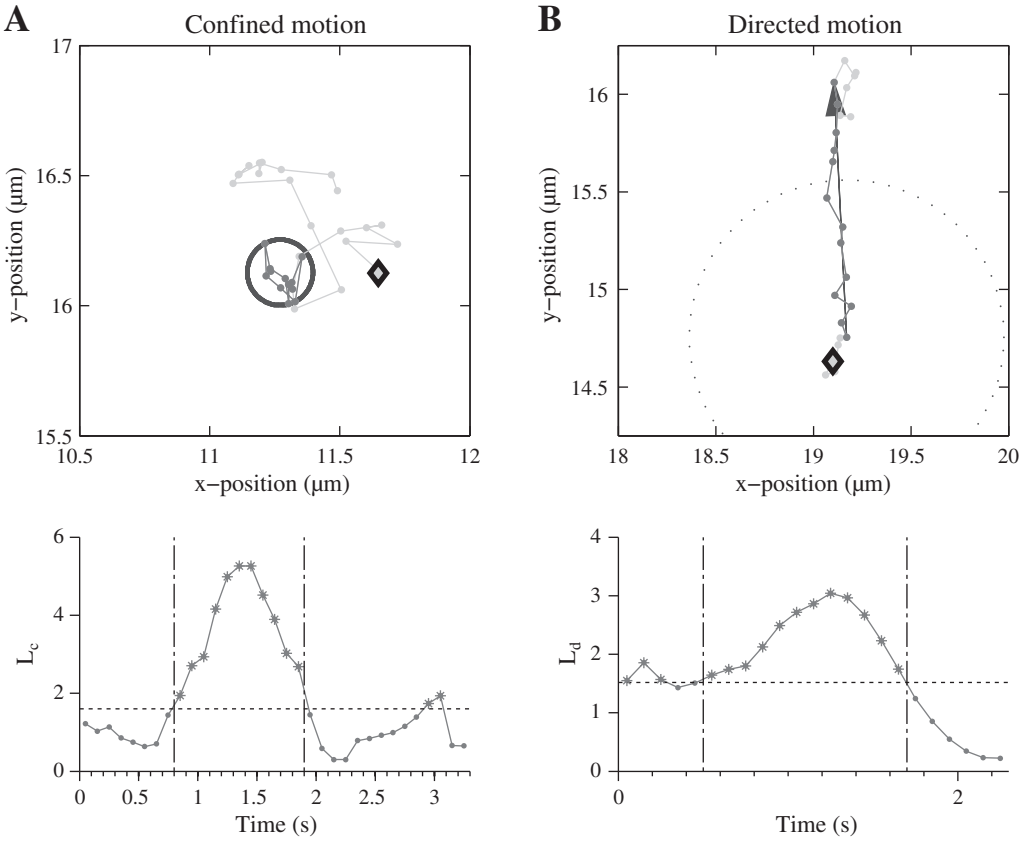

Fig. 2. Identification of anomalous diffusion sections in GlyR trajectories using local displacement analysis. **A**. Detection of confined motion based on the confinement probability level (L_c). **Upper:** Representative trajectory of the GlyR α3 K in HEK 293 cells containing a confinement region (circle). **Lower:** This region was identified by detecting trajectory sections with $L_c > 1.6$ (horizontal line, *) for at least 10 consecutive displacements (vertical lines). **B**. Detection of directed motion (arrow), based on the directed motion probability level (L_d). **Upper:** Representative trajectory of the GlyR α3 L in HEK 293 cells containing directed motion (arrow). The minimum displacement required for directed motion is also indicated (dotted circle). **Lower:** The directed motion was identified by detecting trajectory sections with $L_d > 1.52$ (horizontal line, *) for at least 7 consecutive displacements (vertical lines). The starting point of each trajectory is indicated (◊).

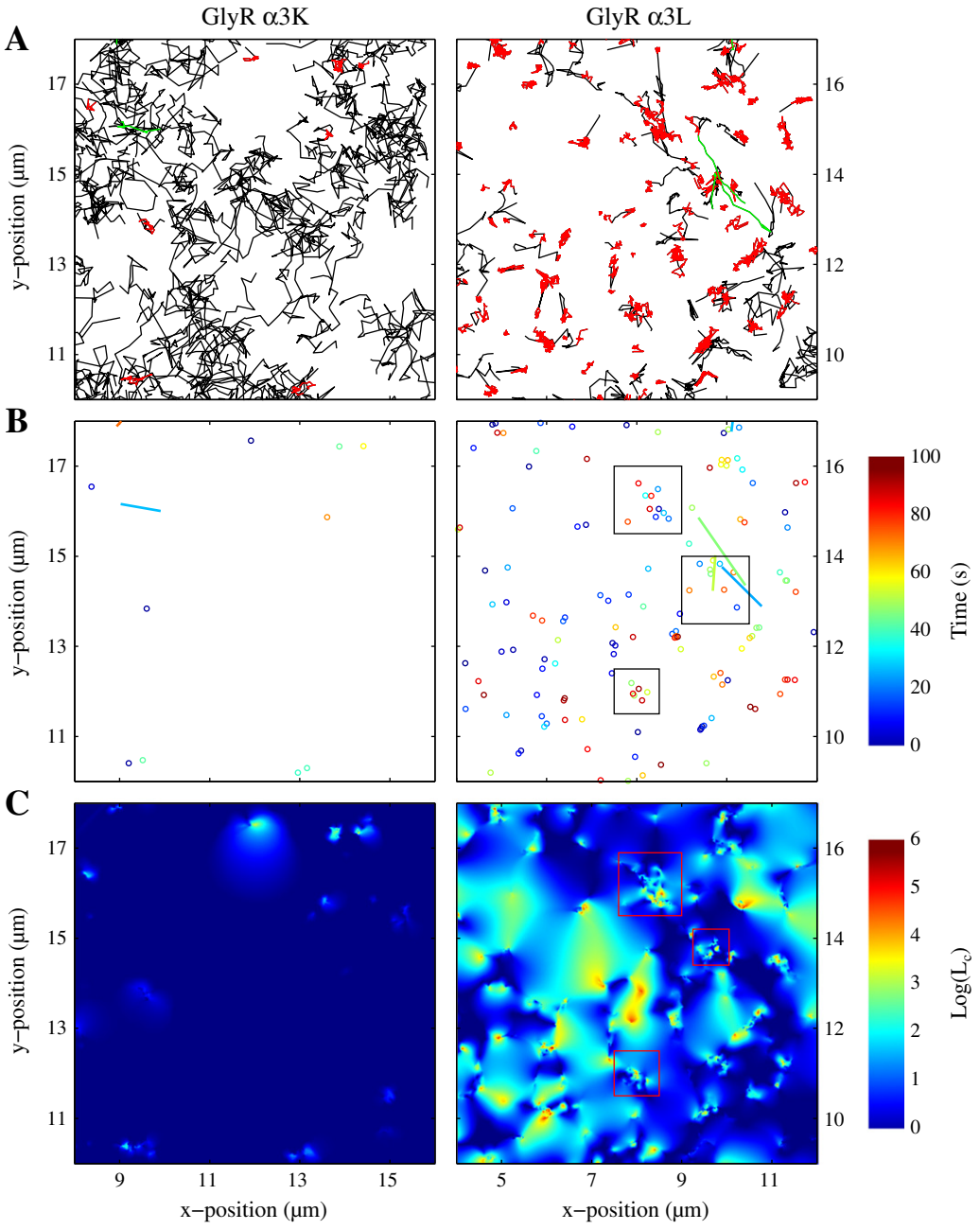

Fig. 3. Visualization of local displacement trajectory analysis in a representative area of the bottom membrane. Identical color coding was used for the α3 K (117 tracks) and α3 L (223 tracks). **A**. Trajectory mapping indicating free diffusion (black), confined motion (red) and directed motion (green). **B**. Mapping of the confined motion (circles) and directed motion events (lines) in time. For confined motion the location represents the centroid of the confinement area. For directed motion, the start and end coordinates of each segment were connected by a straight line. The central frame of the occurrence was used as a time reference. Exemplary membrane areas with reoccurring events are marked by black rectangles. **C**. Mapping of L_c. The center coordinates of all displacements were used and the corresponding log(L_c) values were interpolated over the surface. Exemplary membrane areas showing irregular high intensity patterns of L_c are marked by red rectangles. (L_c = confinement probability level).

Quantitative parameters of the anomalous diffusion events were also determined (Table 1). The average *prevalence* of confined motion was 24 ± 3% for α3 K and was significantly elevated for α3 L with 78 ± 4%. Similarly, the *confined fraction* constituted 20 ± 3% and 74 ± 4% of all displacements for α3 K and α3 L respectively. For each confined motion section *residence time* and ρ were determined. The distributions of *residence time* show a range of 1 s to 6.3 s for α3 K and 1 s to 13.4 s for α3 L. The distribution of *residence time* for the α3L variant is right shifted compared to the α3 K (Fig. 5A). As expected, the average *residence time* is significantly elevated for the α3L variant (2.8 ± 0.1 s), compared to α3 K (1.9 ± 0.1 s). The distributions of ρ range from 0.050 μm to 0.290 μm and 0.046 to 0.341 μm for respectively α3 K and α3 L in HEK 293 cells. (Fig. 5B). These distributions were markedly similar and also the average ρ did not show any significant difference with 0.153 ± 0.004 μm for α3 K and 0.156 ± 0.003 μm for α3 L.

Sections with directed motion were rare compared to sections with confined motion, with a *prevalence* of only 1.1 ± 0.2% for the trajectories described by α3K and 2.7 ± 0.3% for the α3L trajectories. Given the low prevalence, the directed motion could only be quantified adequately for α3L. This was done by calculating the *travel time*, *distance* and *speed*. The process of directed motion was short lived, with an average *travel time* of 1.00 ± 0.04 s and a maximum of 2.4 s. The distribution of *distance* ranged from 0.75 to 4.8 μm, with the average *distance*

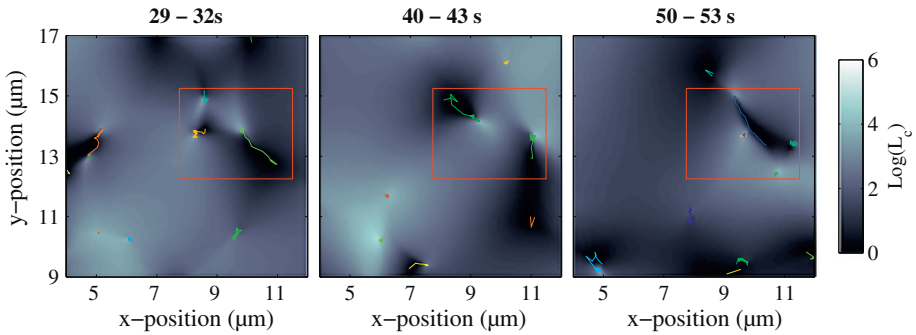

Fig. 4. Visualization of L_c variation during short time intervals. The color map was adapted to improve visibility of the plotted trajectories. Trajectories are individually color coded in each time interval to facilitate distinction. The red box demarcates an area showing high variations in confinement strength occurring in multiple individual trajectories spread over time. (L_c = confinement probability level).

measuring 1.7 ± 0.1 μm (Fig. 5C). The distribution of *speed* at which the directed motion occurred ranged from 0.81 μm/s to 3.5 μm/s, with an average *speed* of 1.77 ± 0.09 μm/s.

Based on the gradients in L_c occurring in individual trajectories, the coincidence of directed and confined motion was assessed (Fig. 6). Directed motion is the least prevalent form of anomalous diffusion and therefore coincidence was calculated as the percentage of trajectories with directed motion, which also contained confined motion. In the α3L GlyR population displaying directed motion, 51 ± 7% also displayed confined motion. The grouped population characteristics of trajectories containing coincident directed and confined motion were further quantified. Both transitions from confined to directed (C – D) and directed to confined (D – C) motion occurred, with an equal 50 ± 12% probability. Furthermore, the transition time (*tt*) was determined by the time span between subsequent events. The average *tt* was 0.15 ± 0.06 s for C – D transitions, while for D – C transitions this was 0.3 ± 0.1 s.

4. Discussion

In this work we elaborate on the presence of anomalous diffusion in α3 GlyR membrane dynamics, as suggested in our earlier report [48]. Further evidence and quantification are obtained by applying advanced analysis of single particle tracking data. Moreover, the anomalous diffusion parameters reveal the nature of the differential dynamics between α3K- and α3L-containing GlyRs. Below, the conclusions are formed by stepwise interpretation of the subsequent analyses and placed in a physiological context.

4.1. Ensemble displacement analysis

In order to explore the heterogeneity of α3 GlyR motion, the populations of displacements were analyzed using a multi-component function [51,54]. For the α3K GlyR displacements, two sub populations of displacement sizes were found, differing more than an order of magnitude. For the first and largest displacement component a linear MSD versus time relationship suggests free diffusion. The diffusion coefficient D_e = 0.13 ± 0.01 μm²/s belonging to this component also corresponds well with previous fluorescence recovery after photobleaching (FRAP) measurements of GlyR α3 K diffusion in HEK 293 cells (0.15 ± 0.01 μm²/s) [48]. The FRAP measurements also reported normal diffusion with a large mobile component (0.93 ± 0.04). The order of magnitude for D_e is also in agreement with values retrieved for extrasynaptic α1-containing GlyRs (0.10 ± 0.01 μm²/s), believed to mainly undergo free diffusion outside the synapse [55]. The smaller second displacement component did not fit to a linear model and corresponds to sub diffusion. The fractions also indicate that the presence of the first component dominates over the second component. This confirms previous assumptions, stating that for α3K GlyRs free diffusion is dominant [48]. The validity of using D_e from α3 K GlyRs as a measure of free diffusion for both variants can be affirmed. The 15 AA difference between the subunit variants, located in the large intracellular loop, is unlikely to influence the radius of the membrane spanning receptor segment, which determines the free diffusion coefficient [5,43,56]. On that premise, the discrepancy between the values of D_e for the two variants likely originates from an expression system-related sampling bias, introduced by applying SPT [48]. Thereby, extracting D_e from the α3 K GlyR was considered more reliable, given the dominant fraction of free diffusion and the less complex nature of diffusion of the α3 K variant. The fact that using D_e from α3 L GlyRs does not change the inference of the local displacement analysis, also shows that the relative difference in D_e between the receptor variants is negligible when considering the full range of diffusion modes.

Table 1
Summary of parameter averages from local displacement analysis of α3 GlyR trajectories from each expression system. For confined motion *residence time*, *confined fraction* and *ρ* are reported. For directed motion *travel time*, *distance* and *speed* are reported. (***: *p*-value < 0.001, NA: Not Applicable).

Motion	Parameters[a]	HEK 293	
		GlyR α3 K	GlyR α3 L
Confined	Prevalence (%)***	24 ± 3	78 ± 4
	Residence time (s)***	1.9 ± 0.1	2.8 ± 0.2
	Confined fraction (%) ***	20 ± 3	74 ± 4
	ρ (μm)	0.153 ± 0.004	0.156 ± 0.003
Directed	Prevalence (%)***	1.1 ± 0.2	2.7 ± 0.3
	Travel time (s)	NA	1.00 ± 0.04
	Distance (μm)	NA	1.7 ± 0.1
	Speed (μm/s)	NA	1.77 ± 0.09

[a] Mean ± standard error (HEK 293 α3 K n = 7, HEK 293 α3 L n = 9).

4.2. Local displacement analysis

Using local displacement analysis, trajectory sections deviating from free diffusion were identified. This strategy optimizes the use of single particle tracking, as anomalous diffusion events can be detected for individual particles [16,22,24]. A confinement probability based on the displacement and a directed motion probability based on the asymmetry properties were calculated [52,57]. Determining the input parameters for the analysis is an empirical process. The analysis is based on short trajectories given the use of a fluorescent dye as label. Furthermore, the approach had to accommodate the spatial and temporal properties of the anomalous processes, while limiting false positive detection.

For the detection of confined motion, the free diffusion coefficient was not estimated from the individual trajectories as done in other work [50], but from the ensemble analysis. In this way, the confined motion was not required to be transient of nature in order to be detected. The previously established presence of an immobile fraction of α3 GlyRs (α3 K: 5%, α3 L: 15%) warranted this approach, as immobile

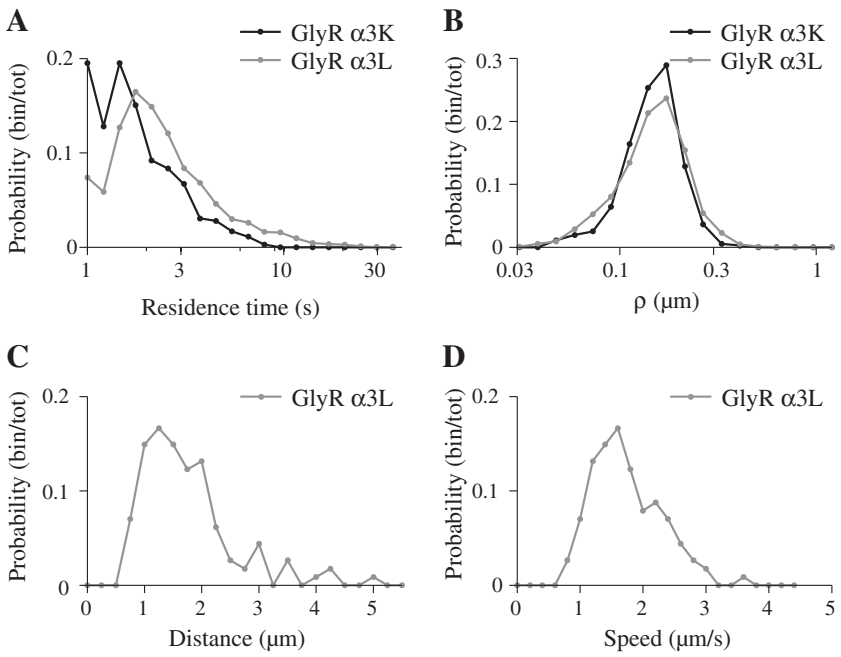

Fig. 5. Quantitative parameters of the anomalous diffusion events. **A**. The distribution (log scale) of the residence times for the confined motion sections. **B**. The distribution (log scale) of ρ for the confined motion sections. **C**. The distributions of the *distance* calculated for all the directed motion sections. **D**. The distributions of the speed calculated for all the directed motion sections. (bin = number of elements in bin, tot = total elements in distribution, ρ = radius of the confinement area).

receptors were considered an extreme case of confined motion [48]. Based on the numerical proximity between the *confined motion prevalence* and the *confined fraction*, on average, confinement is dominant in trajectories containing a confinement zone. As the possibility to discriminate true confinement increases for longer observation times [52], a large sliding window was selected. We also chose to optimize detection of stable confinement zones, therefore setting a high minimally required *residence time* and allowing a less rigorous threshold of L_c to avoid false positives.

Confined motion of the GlyR has been described in most detail for the α1-containing heteromeric GlyRs, as part of a diffusion and trapping model mediated by gephyrin anchoring [35,38,58]. For the heteromeric GlyR α1, binding to gephyrin leads to clustering of the receptor at the synapse [35,59]. However, gephyrin-independent clusters of α1-, α2- and α3-containing homomeric GlyRs have also been established, with clustering of homomeric α3-receptors being shown in both primary neurons and HEK 293 cells [38,44,60]. Here, it is demonstrated that α3 GlyR dynamics also involve a trapping mechanism for local α3 GlyR accumulation. ρ corresponds well to the sub-micrometer clustering found for α3L GlyRs by super-resolution microscopy [48]. Mapping of α3L GlyR diffusion reveals localized diffusion with areas showing high incidence of confined motion. Protein oligomerization, lipid raft association or clathrin-mediated stabilization is a possible mechanism of GlyR trapping in HEK 293 cells, demonstrated previously for other transmembrane proteins [61–64]. With regards to biological signaling, confining receptors in specific membrane areas or in high density clusters can affect both the immediate electrophysiological response as well as the downstream signaling capacity [31,65–67].

Interestingly, the GlyR α3 K is also capable of being confined, yet the frequency and the stability of the confined state are not sufficient for outspoken local accumulation of this variant. The similar range of ρ suggests both variants are prone to the same confining interactions, yet with different efficiencies. Alternatively, α3 L may undergo an additional confining interaction, an argument supported by the increased number of components in the ensemble analysis. In that respect the 15 AA insert of α3 L can either indirectly stabilize interactions, as its absence leads to unstable folding of the large TM 3–4 intracellular domain [45]. On the other hand, the insert can also be a binding target, leading to additional confinement, similar to the gephyrin binding domain of the β-subunit [68].

The determination of directed motion was based on the asymmetry of the gyration matrix **T**, a measure independent of the displacement size. Thereby directed motion was initially independent of the diffusion coefficient and observation time [57]. This allowed a reduction of the sliding window size, making L_d less smooth but more sensitive to short time scale fluctuations. Considering the fast dynamics of directed motion, not dependent on Brownian motion, such a detection scheme was considered advantageous. However, the supposition of directed motion involved an elongated trajectory form [48], displaying a net displacement. As asymmetry is not exclusive to elongated trajectories, incorporating a minimum square displacement improved detection of directed motion. A two parameter (asymmetry and minimum square displacement) detection scheme also allowed for a more efficient discrimination of directed motion from free diffusion.

The low directed motion *prevalence* could in part be attributed to the technical difficulties of tracking a fast moving particle in a heterogeneously diffusing particle population. The presence of micrometer scale saltatory motion at speeds of almost several micrometers per second is not common for transmembrane proteins. It has been reported for vesicular transport guided by motor proteins, which has been established in transmembrane receptor trafficking [69–71]. Vesicular transport by motor proteins is also a means of antero- and retrograde transport in neurons and is essential for GlyR trafficking [30,72–75]. With the TIRF setup it is only possible to monitor vesicular transport near and parallel to the cell membrane, biasing directed motion *prevalence* [76,77]. Regardless of the low prevalence, active (re-)distribution in the membrane is likely to be requisite for α3L GlyRs given their stationary nature. The contrasting mobile nature of α3K GlyRs, might explain the decreased occurrence or absence of directed motion dynamics.

The presence of confined and directed motion being explained by two independent processes is possible, but unlikely in this case. Mapping of the trajectories indicated steep gradients in confinement probability, resembling a transfer of motion type. Therefore the coincidence of directed and confined motion in single trajectories was investigated. Over half of the trajectories exhibiting directed motion also displayed confinement, confirming that a single receptor can be

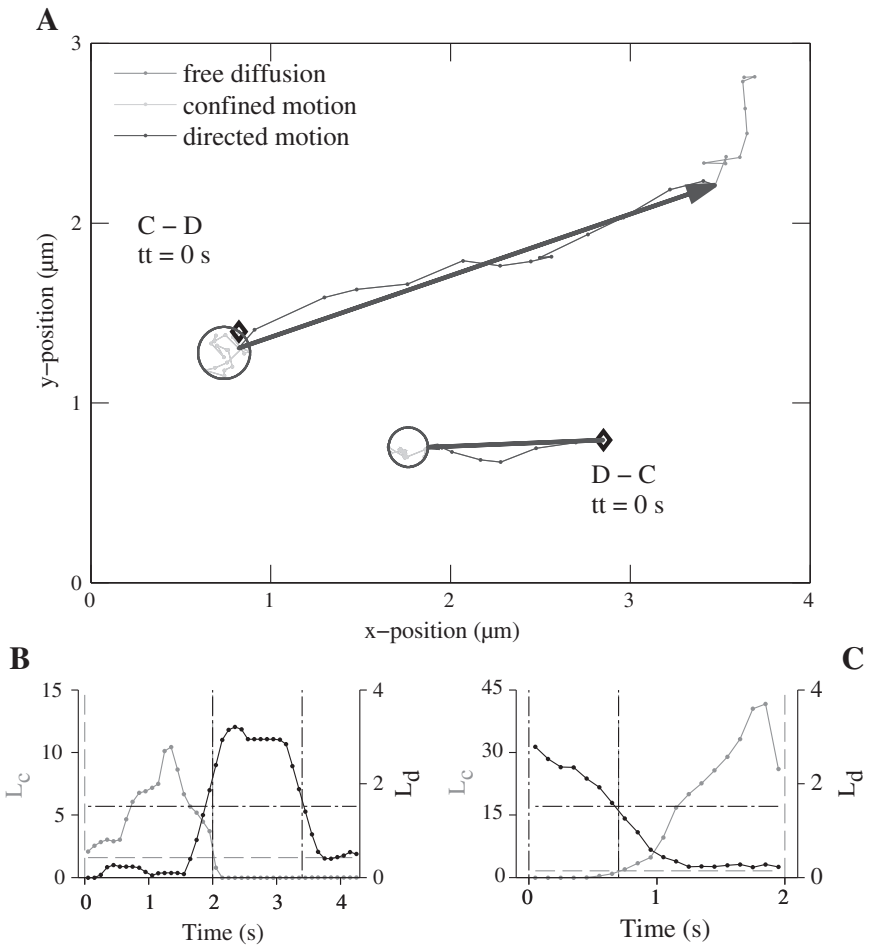

Fig. 6. Two examples of trajectories displaying coincident confined and directed motion. **A**. The GlyR α3L trajectories were analyzed using the local displacement analysis and segmented into free diffusion, confined motion (circle) and directed motion (arrow). The starting point of each trajectory is indicated (◊). **B**. Plot of L_c and L_d over the course of a trajectory showing a confined to directed motion transition (C – D). The thresholds (horizontal lines) and anomalous segments (vertical lines) are indicated. In this case, $tt = 0$, notice that the first displacement exceeding the threshold of L_d is not selected because it also exceeds the L_c threshold. **C**. Plot of the L_c and L_d over the course of a trajectory showing a directed to confined motion transition (D – C). The thresholds (horizontal lines) and anomalous segments (vertical lines) indicate an instantaneous transition. (L_c = confinement probability level, L_d = directed motion probability level, tt = transition time).

subjected to both types of anomalous diffusion. There was no particular order in the occurrence of directed and confined motion. However, analysis of the time span of the transitions indicated that, under the given temporal resolution, the different motion types occurred in almost immediate succession. The occurrence of different motion types in a transmembrane receptor population has been reported before [15,78]. The presence of coupled confined and directed motion, more specifically resembles clathrin-mediated receptor stabilization and dynamin-dependent endocytosis coupled to vesicular receptor trafficking/recycling as described for transferrin, epidermal growth factor receptors and AMPA receptors [63,79–83]. In fact, both α3 RNA splice variants harbor at the N-terminus of the TM 3–4 cytosolic loop a di-leucine motif involved in dynamin (AP-2)-dependent receptor internalization [43,84,85]. Furthermore cargo dependence of dynamin-regulated clathrin-coated pit maturation has been demonstrated [86]. In that respect, the diffuse α3K GlyRs may, in contrast to the accumulating α3L GlyRs, not be capable of producing sufficient cargo for endocytosis. Active removal and recycling of ligand-gated receptors from the membrane are an important means to physiologically modulate their function [87]. Distinct pathways of transmembrane receptor endocytosis have even been shown to differentially impact the signaling cascade [88,89].

To summarize, advanced single particle tracking analysis has revealed new information on the membrane dynamics of homomeric α3-containing GlyRs. The heterogeneous α3 GlyR motion pattern was quantified and interpreted using a combination of ensemble and local SPT analysis. The α3 GlyRs show exchange between states of local confinement and normal diffusion. RNA splicing exerts a major influence on the balance between these states and is associated with directed motion in the case of α3 L GlyRs. The speed of the directed motion matches that of saltatory vesicular motion and frequently occurs coupled to confined motion. These characteristic motion features strongly suggest that molecular interaction between a cellular component and the exon 8A-encoded sequence of the RNA splicing-dependent L-insert (TEAFALEKFYRFSDT) is responsible for directed motion and anomalous diffusion of this GlyR α3 RNA splice variant. Differential desensitization and synaptic clustering of these receptor RNA variants imply that their biophysical membrane behavior strongly impacts GlyR α3 signaling. Consequently these results are also relevant to GlyR α3 pathophysiology in neurological disorders [90], e.g. in temporal lobe epilepsy where GlyR α3 RNA splicing is changed in patients with a severe disease course [44,47].

Acknowledgments

This work was funded by the Research Council of the UHasselt, tUL. GlyR expression constructs were obtained thanks to funding by the Helmholtz Association (VH-NG-246 to J.C.M.) and the Bundesministerium für Bildung und Forschung BMBF (Era-Net NEURON II CIPRESS to J.C.M.). The research leading to these results

has received funding from the European Research Council under the European Union's Seventh Framework Program (FP7/2007–2013)/ERC Grant Agreement n° 291593 FLUOROCODE), from the Flemish government in the form of long-term structural funding "Methusalem" grant METH/08/04 CASAS, from the 'Fonds voor Wetenschappelijk Onderzoek Vlaanderen' (FWO grants G.0197.11; G0484.12,) and from the Hercules Foundation (HER/08/021). S.R., J.H. and M.A. thank the Federal Science Policy of Belgium (IAP-VI/27). The support by the FWO-onderzoeksgemeenschap "Scanning and Wide Field Microscopy of (Bio)-organic Systems" is gratefully acknowledged by J.H. and M.A.

Appendix A. Supplementary data

Supplementary data to this article can be found online at http://dx.doi.org/10.1016/j.bbamcr.2013.11.019.

References

[1] Z.Q. Xu, X. Zhang, L. Scott, Regulation of G protein-coupled receptor trafficking, Acta Physiol (Oxf.) 190 (2007) 39–45.
[2] L. Groc, L. Bard, D. Choquet, Surface trafficking of N-methyl-D-aspartate receptors: physiological and pathological perspectives, Neuroscience 158 (2009) 4–18.
[3] I. Chung, R. Akita, R. Vandlen, D. Toomre, J. Schlessinger, I. Mellman, Spatial control of EGF receptor activation by reversible dimerization on living cells, Nature 464 (2010) 783–787.
[4] S.J. Singer, G.L. Nicolson, The fluid mosaic model of the structure of cell membranes, Science 175 (1972) 720–731.
[5] Y. Gambin, R. Lopez-Esparza, M. Reffay, E. Sierecki, N.S. Gov, M. Genest, R.S. Hodges, W. Urbach, Lateral mobility of proteins in liquid membranes revisited, Proc. Natl. Acad. Sci. U. S. A. 103 (2006) 2098–2102.
[6] P.G. Saffman, M. Delbruck, Brownian motion in biological membranes, Proc. Natl. Acad. Sci. U. S. A. 72 (1975) 3111–3113.
[7] D. Lingwood, K. Simons, Lipid rafts as a membrane-organizing principle, Science 327 (2010) 46–50.
[8] Y. Sako, A. Kusumi, Compartmentalized structure of the plasma membrane for receptor movements as revealed by a nanometer-level motion analysis, J. Cell Biol. 125 (1994) 1251–1264.
[9] K. Ritchie, R. Iino, T. Fujiwara, K. Murase, A. Kusumi, The fence and picket structure of the plasma membrane of live cells as revealed by single molecule techniques (Review), Mol. Membr. Biol. 20 (2003) 13–18.
[10] J. Fantini, F.J. Barrantes, How cholesterol interacts with membrane proteins: an exploration of cholesterol-binding sites including CRAC, CARC, and tilted domains, Front. Physiol. 4 (2013) 31.
[11] M.J. Saxton, Wanted: a positive control for anomalous subdiffusion, Biophys. J. 103 (2012) 2411–2422.
[12] P.R. Smith, I.E. Morrison, K.M. Wilson, N. Fernandez, R.J. Cherry, Anomalous diffusion of major histocompatibility complex class I molecules on HeLa cells determined by single particle tracking, Biophys. J. 76 (1999) 3331–3344.
[13] P.H. Lommerse, G.A. Blab, L. Cognet, G.S. Harms, B.E. Snaar-Jagalska, H.P. Spaink, T. Schmidt, Single-molecule imaging of the H-ras membrane-anchor reveals domains in the cytoplasmic leaflet of the cell membrane, Biophys. J. 86 (2004) 609–616.
[14] P.W. Wiseman, C.M. Brown, D.J. Webb, B. Hebert, N.L. Johnson, J.A. Squier, M.H. Ellisman, A.F. Horwitz, Spatial mapping of integrin interactions and dynamics during cell migration by image correlation microscopy, J. Cell Sci. 117 (2004) 5521–5534.
[15] K.M. Wilson, I.E. Morrison, P.R. Smith, N. Fernandez, R.J. Cherry, Single particle tracking of cell-surface HLA-DR molecules using R-phycoerythrin labeled monoclonal antibodies and fluorescence digital imaging, J. Cell Sci. 109 (Pt 8) (1996) 2101–2109.
[16] M.J. Saxton, K. Jacobson, Single-particle tracking: applications to membrane dynamics, Annu. Rev. Biophys. Biomol. Struct. 26 (1997) 373–399.
[17] F. Daumas, N. Destainville, C. Millot, A. Lopez, D. Dean, L. Salome, Interprotein interactions are responsible for the confined diffusion of a G-protein-coupled receptor at the cell surface, Biochem. Soc. Trans. 31 (2003) 1001–1005.
[18] A. Kusumi, C. Nakada, K. Ritchie, K. Murase, K. Suzuki, H. Murakoshi, R.S. Kasai, J. Kondo, T. Fujiwara, Paradigm shift of the plasma membrane concept from the two-dimensional continuum fluid to the partitioned fluid: high-speed single-molecule tracking of membrane molecules, Annu. Rev. Biophys. Biomol. Struct. 34 (2005) 351–378.
[19] C. Eggeling, C. Ringemann, R. Medda, G. Schwarzmann, K. Sandhoff, S. Polyakova, V.N. Belov, B. Hein, C. von Middendorff, A. Schonle, S.W. Hell, Direct observation of the nanoscale dynamics of membrane lipids in a living cell, Nature 457 (2009) 1159–1162.
[20] D. Alcor, G. Gouzer, A. Triller, Single-particle tracking methods for the study of membrane receptors dynamics, Eur. J. Neurosci. 30 (2009) 987–997.
[21] S. Wieser, G.J. Schutz, Tracking single molecules in the live cell plasma membrane-Do's and Don't's, Methods 46 (2008) 131–140.
[22] C.M. Anderson, G.N. Georgiou, I.E. Morrison, G.V. Stevenson, R.J. Cherry, Tracking of cell surface receptors by fluorescence digital imaging microscopy using a charge-coupled device camera. Low-density lipoprotein and influenza virus receptor mobility at 4 degrees C, J. Cell Sci. 101 (Pt 2) (1992) 415–425.
[23] H. Qian, M.P. Sheetz, E.L. Elson, Single particle tracking. Analysis of diffusion and flow in two-dimensional systems, Biophys. J. 60 (1991) 910–921.
[24] T. Schmidt, G.J. Schutz, W. Baumgartner, H.J. Gruber, H. Schindler, Imaging of single molecule diffusion, Proc. Natl. Acad. Sci. U. S. A. 93 (1996) 2926–2929.
[25] M. Heidbreder, C. Zander, S. Malkusch, D. Widera, B. Kaltschmidt, C. Kaltschmidt, D. Nair, D. Choquet, J.B. Sibarita, M. Heilemann, TNF-alpha influences the lateral dynamics of TNF receptor I in living cells, Biochim. Biophys. Acta 1823 (2012) 1984–1989.
[26] A. Serge, N. Bertaux, H. Rigneault, D. Marguet, Dynamic multiple-target tracing to probe spatiotemporal cartography of cell membranes, Nat. Meth. 5 (2008) 687–694.
[27] S. Wieser, M. Axmann, G.J. Schutz, Versatile analysis of single-molecule tracking data by comprehensive testing against Monte Carlo simulations, Biophys. J. 95 (2008) 5988–6001.
[28] A. Triller, D. Choquet, New concepts in synaptic biology derived from single-molecule imaging, Neuron 59 (2008) 359–374.
[29] D. Choquet, Fast AMPAR trafficking for a high-frequency synaptic transmission, Eur. J. Neurosci. 32 (2010) 250–260.
[30] A. Dumoulin, A. Triller, M. Kneussel, Cellular transport and membrane dynamics of the glycine receptor, Front. Mol. Neurosci. 2 (2009) 28.
[31] J.H. Kim, R.L. Huganir, Organization and regulation of proteins at synapses, Curr. Opin. Cell Biol. 11 (1999) 248–254.
[32] A.J. Borgdorff, D. Choquet, Regulation of AMPA receptor lateral movements, Nature 417 (2002) 649–653.
[33] J. Kirsch, G. Meyer, H. Betz, Synaptic targeting of ionotropic neurotransmitter receptors, Mol. Cell. Neurosci. 8 (1996) 93–98.
[34] H.D. MacGillavry, J.M. Kerr, T.A. Blanpied, Lateral organization of the postsynaptic density, Mol. Cell. Neurosci. 48 (2011) 321–331.
[35] J. Meier, C. Meunier-Durmort, C. Forest, A. Triller, C. Vannier, Formation of glycine receptor clusters and their accumulation at synapses, J. Cell Sci. 113 (Pt 15) (2000) 2783–2795.
[36] B. Zuber, N. Unwin, Structure and superorganization of acetylcholine receptor-rapsyn complexes, Proc. Natl. Acad. Sci. U. S. A. 110 (2013) 10622–10627.
[37] A. Triller, D. Choquet, Surface trafficking of receptors between synaptic and extrasynaptic membranes: and yet they do move! Trends Neurosci. 28 (2005) 133–139.
[38] M.V. Ehrensperger, C. Hanus, C. Vannier, A. Triller, M. Dahan, Multiple association states between glycine receptors and gephyrin identified by SPT analysis, Biophys. J. 92 (2007) 3706–3718.
[39] J.W. Lynch, Molecular structure and function of the glycine receptor chloride channel, Physiol. Rev. 84 (2004) 1051–1095.
[40] J.W. Lynch, S. Rajendra, K.D. Pierce, C.A. Handford, P.H. Barry, P.R. Schofield, Identification of intracellular and extracellular domains mediating signal transduction in the inhibitory glycine receptor chloride channel, EMBO J. 16 (1997) 110–120.
[41] J.W. Lynch, Native glycine receptor subtypes and their physiological roles, Neuropharmacology 56 (2009) 303–309.
[42] R.J. Harvey, U.B. Depner, H. Wassle, S. Ahmadi, C. Heindl, H. Reinold, T.G. Smart, K. Harvey, B. Schutz, O.M. Abo-Salem, A. Zimmer, P. Poisbeau, H. Welzl, D.P. Wolfer, H. Betz, H.U. Zeilhofer, U. Muller, GlyR alpha3: an essential target for spinal PGE2-mediated inflammatory pain sensitization, Science 304 (2004) 884–887.
[43] Z. Nikolic, B. Laube, R.G. Weber, P. Lichter, P. Kioschis, A. Poustka, C. Mulhardt, C.M. Becker, The human glycine receptor subunit alpha3. Glra3 gene structure, chromosomal localization, and functional characterization of alternative transcripts, J. Biol. Chem. 273 (1998) 19708–19714.
[44] S.A. Eichler, B. Forstera, B. Smolinsky, R. Juttner, T.N. Lehmann, M. Fahling, G. Schwarz, P. Legendre, J.C. Meier, Splice-specific roles of glycine receptor alpha3 in the hippocampus, Eur. J. Neurosci. 30 (2009) 1077–1091.
[45] H.G. Breitinger, C. Villmann, N. Melzer, J. Rennert, U. Breitinger, S. Schwarzinger, C.M. Becker, Novel regulatory site within the TM3-4 loop of human recombinant alpha3 glycine receptors determines channel gating and domain structure, J. Biol. Chem. 284 (2009) 28624–28633.
[46] S.A. Eichler, S. Kirischuk, R. Juttner, P.K. Schaefermeier, P. Legendre, T.N. Lehmann, T. Gloveli, R. Grantyn, J.C. Meier, Glycinergic tonic inhibition of hippocampal neurons with depolarizing GABAergic transmission elicits histopathological signs of temporal lobe epilepsy, J. Cell. Mol. Med. 12 (2008) 2848–2866.
[47] P. Legendre, B. Forstera, R. Juttner, J.C. Meier, Glycine receptors caught between genome and proteome - functional implications of RNA editing and splicing, Front. Mol. Neurosci. 2 (2009) 23.
[48] K. Notelaers, N. Smisdom, S. Rocha, D. Janssen, J.C. Meier, J.M. Rigo, J. Hofkens, M. Ameloot, Ensemble and single particle fluorimetric techniques in concerted action to study the diffusion and aggregation of the glycine receptor alpha3 isoforms in the cell plasma membrane, Biochim. Biophys. Acta 1818 (2012) 3131–3140.
[49] N. Meilhac, L. Le Guyader, L. Salome, N. Destainville, Detection of confinement and jumps in single-molecule membrane trajectories, Phys. Rev. E Stat. Nonlinear Soft Matter Phys. 73 (2006) 011915.
[50] R. Simson, E.D. Sheets, K. Jacobson, Detection of temporary lateral confinement of membrane proteins using single-particle tracking analysis, Biophys. J. 69 (1995) 989–993.
[51] G.J. Schutz, H. Schindler, T. Schmidt, Single-molecule microscopy on model membranes reveals anomalous diffusion, Biophys. J. 73 (1997) 1073–1080.
[52] M.J. Saxton, Lateral diffusion in an archipelago. Single-particle diffusion, Biophys. J. 64 (1993) 1766–1780.
[53] L.C. Elliott, M. Barhoum, J.M. Harris, P.W. Bohn, Trajectory analysis of single molecules exhibiting non-brownian motion, Phys. Chem. Chem. Phys. 13 (2011) 4326–4334.
[54] S. Rocha, J.A. Hutchison, K. Peneva, A. Herrmann, K. Mullen, M. Skjot, C.I. Jorgensen, A. Svendsen, F.C. De Schryver, J. Hofkens, H. Uji-i, Linking phospholipase mobility to activity by single-molecule wide-field microscopy, Chemphyschem 10 (2009) 151–161.

[55] M. Dahan, S. Levi, C. Luccardini, P. Rostaing, B. Riveau, A. Triller, Diffusion dynamics of glycine receptors revealed by single-quantum dot tracking, Science 302 (2003) 442–445.
[56] J. Kuhse, V. Schmieden, H. Betz, Identification and functional expression of a novel ligand binding subunit of the inhibitory glycine receptor, J. Biol. Chem. 265 (1990) 22317–22320.
[57] M.J. Saxton, Single-particle tracking: models of directed transport, Biophys. J. 67 (1994) 2110–2119.
[58] J. Meier, C. Vannier, A. Serge, A. Triller, D. Choquet, Fast and reversible trapping of surface glycine receptors by gephyrin, Nat. Neurosci. 4 (2001) 253–260.
[59] J. Meier, R. Grantyn, A gephyrin-related mechanism restraining glycine receptor anchoring at GABAergic synapses, J. Neurosci. 24 (2004) 1398–1405.
[60] R. Bluem, E. Schmidt, C. Corvey, M. Karas, A. Schlicksupp, J. Kirsch, J. Kuhse, Components of the translational machinery are associated with juvenile glycine receptors and are redistributed to the cytoskeleton upon aging and synaptic activity, J. Biol. Chem. 282 (2007) 37783–37793.
[61] U. Schmidt, M. Weiss, Anomalous diffusion of oligomerized transmembrane proteins, J. Chem. Phys. 134 (2011) 165101.
[62] I. Kim, W. Pan, S.A. Jones, Y. Zhang, X. Zhuang, D. Wu, Clathrin and AP2 are required for PtdIns(4,5)P2-mediated formation of LRP6 signalosomes, J. Cell Biol. 200 (2013) 419–428.
[63] E.M. Petrini, J. Lu, L. Cognet, B. Lounis, M.D. Ehlers, D. Choquet, Endocytic trafficking and recycling maintain a pool of mobile surface AMPA receptors required for synaptic potentiation, Neuron 63 (2009) 92–105.
[64] F.J. Barrantes, Cholesterol effects on nicotinic acetylcholine receptor, J. Neurochem. 103 (Suppl. 1) (2007) 72–80.
[65] P. Legendre, E. Muller, C.I. Badiu, J. Meier, C. Vannier, A. Triller, Desensitization of homomeric alpha1 glycine receptor increases with receptor density, Mol. Pharmacol. 62 (2002) 817–827.
[66] P.Y. Law, L.J. Erickson, R. El-Kouhen, L. Dicker, J. Solberg, W. Wang, E. Miller, A.L. Burd, H.H. Loh, Receptor density and recycling affect the rate of agonist-induced desensitization of mu-opioid receptor, Mol. Pharmacol. 58 (2000) 388–398.
[67] E.M. Petrini, I. Marchionni, P. Zacchi, W. Sieghart, E. Cherubini, Clustering of extrasynaptic GABA(A) receptors modulates tonic inhibition in cultured hippocampal neurons, J. Biol. Chem. 279 (2004) 45833–45843.
[68] G. Meyer, J. Kirsch, H. Betz, D. Langosch, Identification of a gephyrin binding motif on the glycine receptor beta subunit, Neuron 15 (1995) 563–572.
[69] C. Bouzigues, M. Dahan, Transient directed motions of GABA(A) receptors in growth cones detected by a speed correlation index, Biophys. J. 92 (2007) 654–660.
[70] J.P. Caviston, E.L. Holzbaur, Microtubule motors at the intersection of trafficking and transport, Trends Cell Biol. 16 (2006) 530–537.
[71] R.D. Vale, F. Malik, D. Brown, Directional instability of microtubule transport in the presence of kinesin and dynein, two opposite polarity motor proteins, J. Cell Biol. 119 (1992) 1589–1596.
[72] N. Hirokawa, R. Takemura, Molecular motors and mechanisms of directional transport in neurons, Nat. Rev. Neurosci. 6 (2005) 201–214.
[73] J.E. Lochner, M. Kingma, S. Kuhn, C.D. Meliza, B. Cutler, B.A. Scalettar, Real-time imaging of the axonal transport of granules containing a tissue plasminogen activator/green fluorescent protein hybrid, Mol. Biol. Cell 9 (1998) 2463–2476.
[74] C. Maas, D. Belgardt, H.K. Lee, F.F. Heisler, C. Lappe-Siefke, M.M. Magiera, J. van Dijk, T.J. Hausrat, C. Janke, M. Kneussel, Synaptic activation modifies microtubules underlying transport of postsynaptic cargo, Proc. Natl. Acad. Sci. U. S. A. 106 (2009) 8731–8736.
[75] C. Maas, N. Tagnaouti, S. Loebrich, B. Behrend, C. Lappe-Siefke, M. Kneussel, Neuronal cotransport of glycine receptor and the scaffold protein gephyrin, J. Cell Biol. 172 (2006) 441–451.
[76] D. Axelrod, Total internal reflection fluorescence microscopy in cell biology, Traffic 2 (2001) 764–774.
[77] S.M. Simon, Partial internal reflections on total internal reflection fluorescent microscopy, Trends Cell Biol. 19 (2009) 661–668.
[78] A. Kusumi, Y. Sako, M. Yamamoto, Confined lateral diffusion of membrane receptors as studied by single particle tracking (nanovid microscopy). Effects of calcium-induced differentiation in cultured epithelial cells, Biophys. J. 65 (1993) 2021–2040.
[79] A.V. Vieira, C. Lamaze, S.L. Schmid, Control of EGF receptor signaling by clathrin-mediated endocytosis, Science 274 (1996) 2086–2089.
[80] S. Felder, K. Miller, G. Moehren, A. Ullrich, J. Schlessinger, C.R. Hopkins, Kinase activity controls the sorting of the epidermal growth factor receptor within the multivesicular body, Cell 61 (1990) 623–634.
[81] S. Chi, H. Cao, Y. Wang, M.A. McNiven, Recycling of the epidermal growth factor receptor is mediated by a novel form of the clathrin adaptor protein Eps15, J. Biol. Chem. 286 (2011) 35196–35208.
[82] E.M. van Dam, W. Stoorvogel, Dynamin-dependent transferrin receptor recycling by endosome-derived clathrin-coated vesicles, Mol. Biol. Cell 13 (2002) 169–182.
[83] F. Huang, A. Khvorova, W. Marshall, A. Sorkin, Analysis of clathrin-mediated endocytosis of epidermal growth factor receptor by RNA interference, J. Biol. Chem. 279 (2004) 16657–16661.
[84] R. Huang, S. He, Z. Chen, G.H. Dillon, N.J. Leidenheimer, Mechanisms of homomeric alpha1 glycine receptor endocytosis, Biochemistry 46 (2007) 11484–11493.
[85] R. Le Borgne, B. Hoflack, Mechanisms of protein sorting and coat assembly: insights from the clathrin-coated vesicle pathway, Curr. Opin. Cell Biol. 10 (1998) 499–503.
[86] D. Loerke, M. Mettlen, D. Yarar, K. Jaqaman, H. Jaqaman, G. Danuser, S.L. Schmid, Cargo and dynamin regulate clathrin-coated pit maturation, PLoS Biol. 7 (2009) e57.
[87] A.C. Magalhaes, K.D. Holmes, L.B. Dale, L. Comps-Agrar, D. Lee, P.N. Yadav, L. Drysdale, M.O. Poulter, B.L. Roth, J.P. Pin, H. Anisman, S.S. Ferguson, CRF receptor 1 regulates anxiety behavior via sensitization of 5-HT2 receptor signaling, Nat. Neurosci. 13 (2010) 622–629.
[88] G.M. Di Guglielmo, C. Le Roy, A.F. Goodfellow, J.L. Wrana, Distinct endocytic pathways regulate TGF-beta receptor signalling and turnover, Nat. Cell Biol. 5 (2003) 410–421.
[89] Z.Y. Chen, A. Ieraci, M. Tanowitz, F.S. Lee, A novel endocytic recycling signal distinguishes biological responses of Trk neurotrophin receptors, Mol. Biol. Cell 16 (2005) 5761–5772.
[90] A. Winkelmann, N. Maggio, J. Eller, G. Caliskan, M. Semtner, U. Häussler, R. Jüttner, T. Dugladze, B. Smolinsky, S. Kowalczyk, E. Chronowska, F.G. Rathjen Schwarz, G. Rechavi, C.A. Haas, A. Kulik, T. Gloveli, U. Heinemann, J.C. Meier, Changes in neural network homeostasis trigger neuropsychiatric symptoms, J. Clin. Invest. (2013), http://dx.doi.org/10.1172/JCI71472.